Materials & Design 228 (2023) 111825

Contents lists available at ScienceDirect

Materials & Design

journal homepage: www.elsevier.com/locate/matdes

# Random networks of disconnected nanoparticles in dielectric layers as a source of electric responsivity

Jacopo Remondina [a,1], Nikita V. Golubev [b], Elena S. Ignat'eva [b], Vladimir N. Sigaev [b], Maurizio Acciarri [a], Alberto Paleari [a,*], Roberto Lorenzi [a]

[a] Department of Materials Science, University of Milano-Bicocca, Via Cozzi 55, 20125 Milano, Italy
[b] P. Sarkisov International Laboratory of Glass-based Functional Materials, Mendeleev University of Chemical Technology of Russia, Miusskaya Square 9, 125047 Moscow, Russia

## HIGHLIGHTS

- A general strategy is described for obtaining hysteretic conductivity and capacitance from charge percolation in disordered networks of nanostructures.
- Electric responsivity in the volt regime is achieved in germanosilicate films with Ga-oxide nanophase thanks to previously unexploited conduction mechanisms.
- Films with Ga-oxide nanostructures are sandwiched between Si substrate and metal electrode giving the first example of nanostructured oxide-in-oxide responsive-MOS.

## GRAPHICAL ABSTRACT

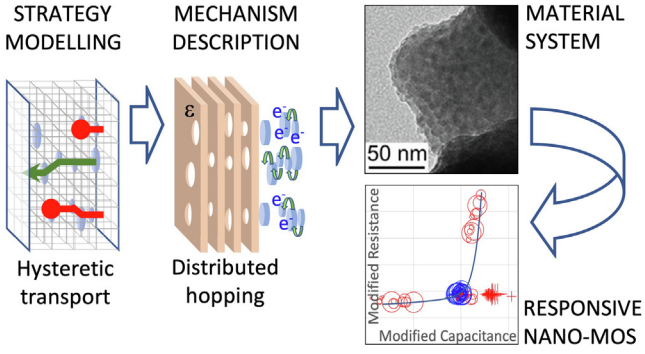


## ARTICLE INFO

*Article history:*
Received 5 December 2022
Revised 3 March 2023
Accepted 10 March 2023
Available online 15 March 2023

*Keywords:*
Inorganic functional materials
Nanostructured materials
Electrical responsivity
Oxide layers
Ga-oxide nanocrystals

## ABSTRACT

Many efforts are currently focused on materials with responsive features for neural-inspired devices. Different approaches are followed, based on various mechanisms – from ferroelectric switching to structural phase changes, from magnetic tunnel junctions to metal filament formation. Here we analyze an alternative strategy based on an unconventional electrical response arising from percolative charge transport and charge trapping in discrete random networks of oxide nanostructures in a dielectric matrix. After an analysis of the mechanisms which can potentially be a source of a plastic response in this class of systems, we report evidence of this behavior in a system comprising an alkali-germanosilicate amorphous matrix with incorporated Ga-oxide nanostructures. The active material – consisting in a film 70 nm thick interfaced to p-type Si and Au electrodes – gives a responsive behavior to pulsed bias which is accompanied by bias dependent electric conduction, with resistivity changes of an order of magnitude by applying 2 V, as well as a dielectric response with hysteretic features, as expected by the model. The results represent a first proof of concept of an unexplored strategy for the design of responsive systems.


## 1. Introduction

Materials with responsive features are actively investigated for opening new perspectives in the design of impactful and energy saving systems for Big Data applications [1–4]. In this field, highly synergetic features of simultaneous storage and processing of

* Corresponding authors.
*E-mail address:* alberto.paleari@unimib.it (A. Paleari).
[1] Present address: Aix-Marseille University/CNRS, IM2NP, Faculté des Sciences de Saint-Jérôme case 142, F-13397 Marseille, France.

https://doi.org/10.1016/j.matdes.2023.111825
0264-1275/

information are required, well beyond what the computing architectures of current microelectronics can now offer. Achieving the target of new brain-inspired computing networks for Artificial Intelligence architectures requires materials whose responsive properties permit to combine memory functions and signal processing, and to obtain memory cells and processing units in a single chip [5].

Main material strategies are based on the use of systems displaying electric field switchable properties such as ferroelectricity or electric conduction. As regards ferroelectricity, information can be stored as electric field switchable polarization in technological systems, provided that a stable and feasible response is obtained in an easily engineerable ferroelectric material, as recently achieved in hybrid-organic–inorganic molecular ferroelectrics [6,7]. As regards electric-field switchable conduction properties, suitable materials are expected to involve conductive paths which can be built up and controlled by the electric signal itself thanks to charge trapping or defect-mediated processes [5–16], or through conductive bridging driven by metal nanostructure forming/dissolving mechanisms inside a dielectric matrix [17–23]. No detailed work is instead reported on responsive features exploiting hopping charge percolation via oxide nanoparticle networks possibly tunable by switching on and off the conductive paths by nanostructure charging under electric signal.

The latter kind of charge transport process is indeed reported to occur in oxide-in-oxide nanostructured materials in which wide-band-gap semiconductors – more specifically, $SnO_2$ or $Ga_2O_3$ – are incorporated in a dielectric amorphous oxide matrix in form of partially conductive nanoparticles [24–27]. These materials display evidence of hysteretic capacitance *vs.* applied voltage, parallel to the occurrence of barrier-limited hopping-mediated charge transport across the nanostructured material. The concomitant charging processes and charge percolating hopping transport – as registered, respectively, by capacitance hysteresis and thermally activated conductance – make these systems potential candidates for a responsive electric behavior. This largely unexplored approach to responsive materials could indeed open the way to the design of a wider class of potential responsive systems.

Aim of the present work is to analyze the feasibility of responsive systems based on a previously unexploited design strategy which takes advantage from competitive mechanisms of nanostructure charging and charge hopping between nanoparticles. The investigation includes the modelling of the expected mechanisms and the analysis of a real nanostructured system consisting in a thin film of amorphous alkali-germanosilicate with incorporated disconnected lenticular nanoaggregates of Ga-oxide. The resulting conductance and capacitance response are measured – either under pulsed electric stimulus or during static electric stress – in a prototype of MOS device comprising the above-mentioned nanostructured system, to collect a proof of concept of responsive systems according to the new strategy.

## 2. Models and methods

### 2.1. Nanostructures as a source of responsivity

The conditions for a responsive electric behavior in a nanostructured oxide-in-oxide material can emerge from two co-occurrences which can potentially be tailored in nanostructured dielectrics. The first one is charge percolation via nanoparticle-mediated charge hopping across the dielectric matrix under an applied electric field $E$. The second circumstance is a suitable level of dispersion of nanostructure features, such as the inter-nanoparticle distance along $E$.

In such a case, the $E$-dependent charge percolation proceeds through conductive steps which display a statistical distribution of the parameters responsible for the nanoparticle-to-nanoparticle charge transfer mechanisms. These can give rise either to an efficient charge transfer between steps along a percolation channel, or to nanoparticle charging if the charge draining from a nanoparticle is less effective than the charge input so that the involved conduction path behaves, to some extent, as a dead-end. The balance between the two mechanisms, and the resulting electric response, depend on the distribution among "easy" and "hard" conduction steps (with efficient or poor charge transfer) in the inhomogeneous percolation network.

Therefore, the distribution of conduction parameters within the network activates a conduction process that can intrinsically have the potential of influencing the conduction channels. This can happen in any step of the network by building up local electrostatic barriers which can in turn be lowered by suitable electric stresses. The local potential barrier to the hopping process by nanoparticle charging can in fact be reduced by charge depletion induced by an electric stimulus. Importantly, the percolative and inhomogeneous conduction not only causes a non-linear $E$-dependence, but also allows the transmitted electric signal to modify the electric conduction itself, thus making the material a responsive system.

### 2.2. Charge transfer in nanostructured chains

We can describe the single $i$-th path across the nanostructured layer by representing it as a sequence of hopping steps in the direction of the electric field. Each step involves a nanostructure with a conduction band suitable to receive, accumulate, and loose charge carriers during the electric conduction. Each step on the $m$-th site of the chain (with $m$ from 1 to $M_i$, where $M_i$ is the number of nanostructures along the $i$-th chain) is influenced by local features – e.g. the distance $r_m$ between neighboring nanostructures and the energy depth $U$ of the electronic states with respect to the localization barrier height – and by external factors, mainly the temperature $T$ and the applied electric field $E$. Whilst $T$ determines the thermal activation of the hopping process, the field $E$ makes the process asymmetric along the field with an energy disproportion between adjacent sites. Furthermore, charge accumulation in the conduction steps – resulting from the charge transport itself – gives rise to electrostatic barriers.

In summary, the charge transfer rate $k_i$ turns out to be described by a term $\exp(-W/k_BT)$, [28–32] where $k_B$ is the Boltzmann constant and $W$ an activation energy which includes $U$, $E$, and $r_m$ and an electrostatic term arising from the charge $q_m$ and $q_{m+1}$ on the involved sites. A quite generic form of the hopping rate $k_{m,m+1}$ from site $m$-th to site $(m + 1)$-th can therefore be written as.

$$k_{m,m+1} = k_0 exp\left[-\left(U_i + eE \cdot r_m + \frac{e}{4\pi\varepsilon}\left(\frac{q_{m+1}}{r_m} - \frac{q_m}{a/2}\right)\right)/k_BT\right] \qquad (1)$$

where the pre-exponential factor $k_0$ determines the low temperature limit of the electron transfer rate, and $a/2$ is the radius of the $m$-th nanostructure. The dot product between $E$ and $r_m$ (the latter with the direction of the hopping step favored by the electric field) and the electrostatic term (with two contributions from the charge on the involved sites) are both responsible for the asymmetry between $k_{m,m+1}$ and $k_{m+1,m}$ at applied $E$ and non-null charge occupation number $n_m$ of each site along the conduction channel.

The hopping rate $k_i$ along the $i$-th channel (with $M_i$ steps) and the accumulated charge $q_i = \Sigma q_m$ (where $q_m = en_m$) on the nanostructures – the former determines the resulting conductivity of the channel, the latter defines the amount of electric dipole built up on the nanostructures – can be derived from $M_i$ kinetic equations for the charge occupation number $n_m$ [29,30]:

$$\frac{dn_m}{dt} = -(k_{m,m+1} + k_{m,m-1})n_m + k_{m-1,m}n_{m-1} + k_{m+1,m}n_{m+1} \quad (2)$$

In steady state conditions ($dn_m/dt$ = 0), with constant charge source and ideal sink at the opposite electrodes ($n_0$ = constant, $n_{Mi}$ = 0), Eq.2 gives a simple expression of the $E$-dependence of the channel rate $k_i$ and the accumulated charge $q_i$. The $E$-dependence of $k_i$ – which in turn determines the $E$-dependence of the electric current $I_i$ along the channel and the related resistance $R_i$ (proportional, respectively, to $k_i$ and 1/ $k_i$ [30]) – is mainly controlled by the change of sign of the term exp(-$E$·$r_m$) between the forward and backward hopping rate $k_{m,m+1}$ and $k_{m+1,m}$ and by the changes of the Coulombic barrier caused by the charge state of the involved sites. One can obtain Marcus's expression in which $k_i$ is a function of all $k_{m,n}(E,q_m,q_n)$ [30] and each $k_{m,n}$ contains $E$-dependent and $q_m$-dependent terms (see Supporting Information and Figure S1 for the case $M$ = 4).

Equation (2) (at $dn_m/dt$ = 0) also gives an expression for $q_i$ = -$\Sigma q_m$ = $e\Sigma n_m$ – where the accumulated $q_m$ on the $m$-th site depends on the unbalanced incoming and outgoing charge – as a function of the hopping rates $k_{m,m+1}$, $k_{m+1,m}$, $k_{m,m-1}$ $k_{m-1,m}$ and the occupation numbers $n_{m-1}$ and $n_{m+1}$:

$$q_m = e\frac{n_{m-1}k_{m-1,m} + n_{m+1}k_{m+1,m}}{k_{m,m-1} + k_{m,m+1}} \quad (3)$$

The $E$-dependence of $k_i$ and $q_i$ can be the source of a non-linear and possibly responsive electric response of the whole nanostructured system. For an easy comparison with experiments, it is useful to express the resulting response as the emergence of a specific $E$-dependence of the resistance and capacitance. In this regard, the present schematic description of a nanostructured system looks at the nanostructures as the hopping steps of a conduction process and, at the same time, as the sites where charge can be accumulated to some extent.

### 2.3. Expected response

As regards the charge transport, each $i$-th conduction channel is characterized by a resistance contribution $R_i$ proportional to $1/k_i$, whilst charge accumulation potentially contributes to a channel capacitance $C_i$ either by charging polarizable trapping sites or giving rise to nanosized dipoles by accumulating injected charges in semi-delocalized nanostructure states. The $E$-dependence of the resulting $R$ and $C$ values of resistance and capacitance of the whole nanostructured system is related to the $E$-dependent $k_i$ and $q_i$ of each $i$-th conduction path and to the total number $N$ of parallel paths across the material. Simplifying the system as a set of $N$ transport channels describable by$\langle k_i^{-1}\rangle$and$\langle q_i\rangle$mean values (see Supplementary Information and Figure S2 for the approximation with $\langle k_i^{-1}\rangle$), we can write the resulting resistance and capacitance as.

$$R(E) \propto \langle k_i^{-1}\rangle/N,\ C(E) \propto N\langle q_i\rangle \quad (4)$$

From Eqs. (1), 3 and 4 – no matter how much more detailed the expressions can become in the specific system one intends to describe – two general facts can be highlighted. On the one hand, the system resistance is expected to decrease nonlinearly with $E$. This is the result of the $E$-dependent exponential term in the hopping rates which accounts for the lowering of the electrostatic barrier along $E$ with respect to the opposite side. On the other hand, the charge accumulated in the nanostructures – potentially acting as incorporated electric dipoles – decreases by increasing the electric field. This is the result of the draining effect of the increase of hopping rate by increasing $E$ against the electrostatic potential initially grown by the charge accumulated in the "hard" steps of the conduction channels. Fig. 1 shows the expected behavior of $R$ and $C$ (represented as normalized quantities proportional to $1/k$ and $q$, respectively) at increasing applied voltage in a simple model comprising a single chargeable four-step conduction channel (see SI). The values are obtained by recursively calculating $k$ and $q$ from starting null input $q$ value (no initial accumulated charge) and subsequent evaluation of modified $q$ (from Eq. (3)) and modified $k$ (from Eq. (1)) at non null $q$ values. It is worth noting that a hysteretic response arises (insets in Fig. 1) provided that inhomogeneous features occur in the system with a distribution of some parameter in the charge transport mechanism, such as the nanostructure-to-nanostructure step distance $r_m$.

In fact, the hysteretic behavior in Fig. 1 disappears when all $r_m$ are equal along the chain. A random distribution of nanostructure sizes and reciprocal distances can be the source of additional responsive properties through remanence effects at zero bias by a not complete reversibility of the discharging process along the hysteretic cycle. When the distribution of nanostructure features is large enough to give rise to retention of charge at null bias, both capacitance and resistance are affected. The dead ends of the conductive path are not fully restored to the initial charge state at null field, and this gives a remanent contribution to $C$ and an increase of $R$ with respect to the pristine value. Analogously, starting from a partially charged starting condition, a hysteretic cycle can bring to a lower charge state with a decrease of $C$ and a resistance $R$ lower than before. The responsive change of state is expected to give rise to an interdependent relation between remanent $C$ and $R$ values. In fact, the larger the remanent charge at some conduction channel – and the resulting capacitance contribution too – the higher the Coulombic barrier against conduction along the channel.

An analytical form describing this effect can easily be written when every electrostatic barrier by remanent charge removes the corresponding nanostructure chain from the ensemble of available conduction channels at null bias. In this approximation, in fact, the $n$ charged channels (out of $N$) give additive contributions to the system capacitance $C$ but, as regards conduction, they are indeed blocked channels. Therefore, the system conductance $R^{-1}$ takes only advantage from the $N$-$n$ parallel contributions of the depleted unblocked channels:

$$C = C_m + \sum_{i=1}^{n} C_i R^{-1} = R_m^{-1} + \sum_{j=1}^{N-n} R_j^{-1} \quad (5)$$

where $C_m$ and $R_m$ are constant contributions from the matrix. The expected relation between $C$ and $R$ along the varieties of possible charged states can be modelled simplifying (as in Eq. (4)) the sums in eq. (5) using the mean values $\langle C_i\rangle$, $\langle R_j\rangle$, and the number $n$ and ($N$-$n$) of involved channels:

$$R^{-1} = \left[R_m^{-1} + \langle R_j\rangle^{-1}\frac{N\langle C_i\rangle + C_m}{\langle C_i\rangle}\right] - \left[\langle R_j\rangle^{-1}\frac{1}{\langle C_i\rangle}\right]C \quad (6)$$

Equation (6) gives a first method to verify the occurrence of a charge transport mechanism involving opening/blocking of conduction channels in a percolative network. As an example, in fact, Fig. 2 shows representative curves of the expected mutual relation between remanent resistance $R$ and remanent capacitance $C$ after stimulus, from Eq. (6), normalized by the pristine $R_0$ and $C_0$ values. Different curves in Fig. 2 reflect different starting conditions before the stimulus in a range comprised between the limit case of all nanostructure chains blocked by charge accumulation – maximum starting values of capacitance and resistance (high $a/b$ value in Fig. 2) – and the opposite limit with almost all chains depleted and available for charge transfer – minimum starting values $R_0$ and $C_0$ (supposing a system with a maximum of about 10% of the system capacitance potentially arising from blocked chains of charged nanostructures).

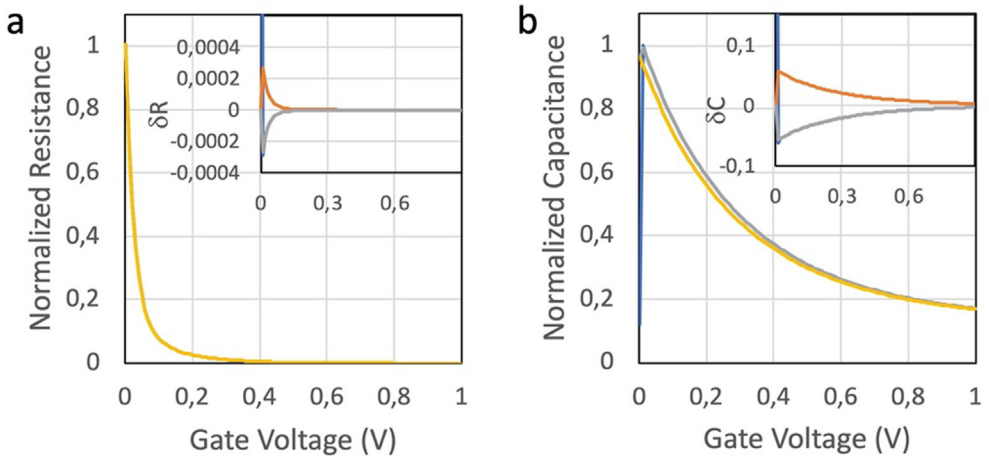


**Fig. 1.** Calculated electric response *vs*. applied voltage *V* in a simplified model of nanostructured system (Fig. S1) at increasing (blue curves), then decreasing (yellow curves) bias, and again (grey curves) in a second ramp at increasing bias (only one color is shown when the curves are visually overlapped). The normalized quantities on the vertical axis are proportional to the *E*-dependent contributions of (a) the inverse charge transfer rate $1/k$ and (b) the accumulated charge *q*, recursively calculated from Eqs. (1) and (3) along cycles of increasing and decreasing applied voltage. Insets: difference between values calculated along the second ramp at decreasing bias and values along the first ramp at increasing bias (blue and grey curves, largely overlapped), and difference between values along the third ramp and the second ramp (orange curves). (For interpretation of the references to color in this figure legend, the reader is referred to the web version of this article.)

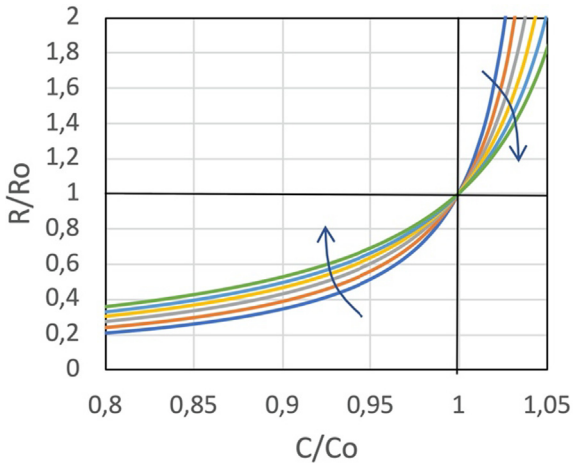


**Fig. 2.** Calculated results of the expected mutual relation between normalized *R* and *C* values resulting from competitive mechanisms of transport blocking within conduction channels after nanostructure charging. Different curves correspond to different choices of *a* and *b* values in the expression $y^{-1} = a\text{-}bx$, from Eq. (6), in the range $1.05<(a/b)$ less than 1.10 according to the arrows pointing to increasing $a/b$ value.

Along these curves, a nanostructured system can display a plastic electric response through the effects of an electric stimulus to the subsequent properties of charge transfer and charge accumulation.

### 2.4. Materials and methods

Several materials could in principle match the structural requirements expected to have a potential for an unconventional and responsive electric behavior. However, the details of the nanostructured features enabling this kind of behavior cannot be defined in general, since they greatly depend on several material parameters related on the specific composition, including the electronic energy structure of nanophase, matrix, and interphase. Evidence of materials with electric functions strongly dependent on the nanostructure features – including nanoparticle interphase and distribution – can be found in the literature, mainly on metal-doped or semiconductor-doped systems, especially in form of hybrid organic–inorganic materials [15,19,33–36]. As regards fully inorganic oxide-in-oxide materials, a system with structural and electronic features potentially resembling the simple model sketched above has recently been characterized in a mixed oxide belonging to gallium-containing amorphous alkali-germanosilicate compounds, specifically in nanostructured films with nominal composition $7.5Li_2O$-$2.5Na_2O$-$20Ga_2O_3$-$25SiO_2$-$45GeO_2$ mol%. In this system, Ga-oxide segregates in disconnected nanostructures incorporated in an amorphous matrix, as observed in bulk [37]. This system undergoes segregation of a Ga-oxide nanophase also when the material is deposited by sputtering on planar substrates, as verified through grazing-incidence x-ray diffraction, small-angle x-ray scattering, atomic-force-microscopy, x-ray reflectivity, and scanning-electron microscopy with Energy-Dispersive x-ray spectroscopy [26,27]. In this case, the nanostructures take lenticular shape, with thickness of the order of $10^1$ nm and lateral size ranging from $10^1$ to $10^2$ nm in diameter [27]. As a result, films 70–100 nm thick give rise to nanostructured layers which contain chains of stacked nanostructures along the direction orthogonal to the film surface, each comprising a small number of disconnected nanoparticles. Furthermore, in this mixed oxide, both the structural peculiarities of Ga-oxide spinel (with octahedrally coordinated Ga sites coexisting with tetrahedral sites [38]) and the coordination structure difference between Ga-oxide and amorphous germanosilicate (mainly tetrahedrally coordinated) give rise to spontaneous deviation of stoichiometry, mainly as oxygen vacancy defects, both within the nanostructures and at the nanoparticle interface and between Ga-oxide spinel nanophase and surrounding germanosilicate glass. Therefore, as observed at the interface of other Ga-containing oxide layers [39], the interface of the incorporated Ga-oxide nanoparticles is naturally enriched by defects and shallow electronic levels, which are mainly donor sites in $Ga_2O_3$ [40,41], providing the nanophase with adequate features for driving charge transfer processes across the material and nanoparticle polarization. The material matches, to some extent, suitable features for giving a nanostructure-driven electric responsivity.

Its structure is representable as a dielectric layer with nanoparticles with electrical conductivity higher than in the host matrix, eventually constituting chains of chargeable and dischargeable

steps along an electric field applied normally to the film interfaces (Fig. 3).

In this work, films of this oxide have been deposited on p-type silicon – by radiofrequency magnetron sputtering and $N_2$ as carrier gas – and capped with a gold electrode to build up a nanostructured MOS device (see Supplementary Information for further experimental details). The next sections report the results collected on a nano-MOS structure with this material, evidencing a response which resembles the behavior modelled in the previous sections.

## 3. Results and discussion

### 3.1. Hysteretic charge transport and charge accumulation

Fig. 4 exemplifies the results of charge transport and charge accumulation in nanostructured MOS with $Ga_2O_3$-in-glass film. The two graphs show the system resistance *R vs.* gate potential *V* and the system capacitance *C vs. V* in the range 0–3 V at both positive and negative bias.

Both curves register a response with some peculiarities with respect to standard MOS systems. The resistance shows a strong bias dependent decrease both at positive and negative gate voltage, which evidences that the oxide layer does not work as a pure dielectric. A previous study indeed clarified the occurrence of conduction through variable hopping and barrier limited mechanisms [26,42–45]. The resistance curve displays an electric-stress induced change of regime with a decrease of an order of magnitude in 2 V. Interestingly, the approximately exponential decrease at increasing bias appears to match the dependence modelled in Fig. 1 for an electric field driven conduction in a nanostructured system.

As regards the capacitance data in Fig. 4, the results appear to qualitatively resemble the usual *C-V* curve of a MOS structure with a p-type semiconductor substrate, showing an inversion region at positive *V* and an accumulation region at negative bias (see Supplementary Information). However, a more detailed insight evidences an anomalous behavior in the *C-V* curve too, with the accumulation region showing a bump, instead of a monotonic behavior towards an asymptotic $C_{ox}$ value, and an overall capacitance largely deviating from the geometric capacitance $C_{ox}$ of the oxide layer.

Besides the anomalies just registered, it is worth noting that both resistance and capacitance display a hysteretic behavior. In fact, analyzing in more details *R* and *C* data collected at increasing and decreasing bias along repeated cycles of applied electric field, differences are registered at equal *V* between ascending and descending ramps (Fig. 5).

Interestingly, differences are mainly observed at small *V*, when the electric field is less effective in smoothing the distribution of easy and hard conduction steps across the nanostructured layer. The results in Fig. 5 indeed match the qualitative behavior modelled in the insets of Fig. 1 for a field-driven conduction in a nanostructured system. Specifically, the results in Fig. 5 show lower *R* and *C* values when the system is coming from higher applied voltage than from smaller *V* values.

As regards the hysteretic resistance, lower *R* at decreasing *V* points to a larger number of low-*R* conduction channels than at increasing *V*. Therefore, the material coming from higher applied field in descending ramp undergoes an electric stress able to unblock conduction paths in which charge accumulation has previously built up an electrostatic barrier during ascending ramp. Furthermore, it is to be noted that the hysteretic response is more evident at negative gate bias, when the charge transport is mainly driven by injection of electrons from the metal, as expected from n-type conduction within the nanostructured film, whilst a more pronounced hysteretic response at positive bias would be expected if p-type conduction were dominant. The results are in fact consistent with the reported n-type nature of Ga-oxide, caused by the native occurrence of donor levels in oxygen vacancy sites.

The hysteretic features of the capacitance can be analyzed in the framework of a MOS structure, provided that the occurrence of charge transport channels and nanostructure charging is accounted for within the oxide layer. In the accumulation regime – at negative bias – the only contribution to the system capacitance comes from the nanostructured oxide layer. However, when the applied bias transforms a relevant portion of the layer in conductive channels across the oxide, only a fraction of the oxide really works as a dielectric. Its capacitive response is therefore reduced with respect to a homogeneous MOS system. This effect can be interpreted, in a first approximation, as a reduction of the effective surface of the nominal dielectric layer. In other words, when the bias is high enough to overcome the Coulombic barrier along a non-negligible fraction of hopping-connected pillars of nanostructures, the dielectric layer can be represented as a capacitor with a surface reduced by a portion as large as the average cross-sectional area per nanostructure multiplied by the concentration per unit area of nanostructures belonging to conductive paths. Since the mean nanostructure size in the investigated material is about $10^2$ nm (corresponding to a cross-sectional area of the order of $10^{-14}$ $m^2$), and the concentration of nanostructures per unit area is of the order of $10^{13}$ $m^{-2}$ (considering $10^3$ nanostructures in a square of about 10 μm in size [27]), thus the upper limit of reduction of the effective dielectric oxide area can be a relevant fraction of the nominal surface. This appears supported by the experimental *C-V* curve, since the capacitance $C_{ox}^{exp}$ in accumulation regime (about 24 nF) deviates significantly from the geometric capacitance $C_{ox}^{geo}$ of the oxide layer. The latter value is in fact expected to be (see Supporting Information) 73 nF starting from the nominal values of layer thickness (70 nm) and dielectric permittivity ($\varepsilon_r$ = 11.6, [46]) of the mixed oxide. Other possible concomitant factors could contribute to this discrepancy, including the growth of thermal oxide at film interfaces. However, a relevant role of the formation of conduction channels parallel to the dielectric portion of the oxide layer is also supported by the experimental $C_{inv}^{exp}$ value of capacitance in inversion regime at positive bias (about 17 nF). This value is in fact anomalously close to the high frequency depletion layer capacitance $C_{DL}^{HF}$ – basically dependent on the features of the p-type Si substrate (see Supporting Information) – which is expected to be 17 nF from the nominal acceptor concentration of the Si substrate (of the order of $10^{16}$ $cm^{-3}$). This result points to the formation, at increasing bias, of a relatively low resistance channel in parallel to the oxide capacitance at increasing bias, as supported by the data in Fig. 4 which show that *R* falls below $10^2$ Ω – less than 10% of the capacitive contribution to the oxide impedance – by applying less than 1 V. In this condition, the whole interface current is shunted to the gate across the oxide and the system approaches, at positive bias, the capacitance response of the depletion layer. From the considerations above, the two limit *C*-values in inversion and accumulation conditions can be taken as representative of the capacitance response of the nanostructured MOS when a large fraction of the conductive channels across the layer is unblocked by the applied bias, and the accumulated charge on the nanostructures is minimized. In this case, the expected *C-V* curve is the result of the response of a modified oxide layer at negative bias –like a capacitor with reduced effective area – and a response at positive bias dominated by the depletion layer alone.

In this framework, the analysis of the differences between the experimental *C-V* curve and the expected behavior in an unblocked nanostructured MOS at intermediate bias can give information on the processes taking place when the nanostructured MOS deviates from the unblocked conditions. In fact, the contribution of nanostructure charging to the formation of nanostructure dipoles can

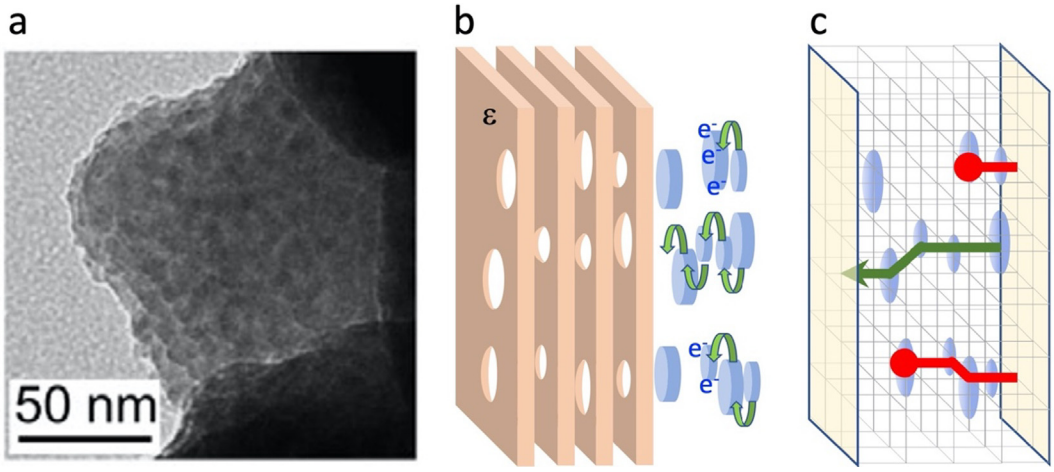


**Fig. 3.** (a) TEM image of Ga-oxide alkali-germanosilicate glass with Ga-oxide nanostructures in the amorphous matrix. (b) Schematic exploded view of the material structure comprising pillars of disconnected nanosystems (blue disks) stacked across the film in a dielectric matrix (holed brown layers), sustaining both charge transport (green arrows) and charge accumulation (represented by $e^-$). (c) Schematic view of the resulting conduction channels (green paths) and charged dead ends (red branches) within the network of steps available for charge transfer. (For interpretation of the references to color in this figure legend, the reader is referred to the web version of this article.)

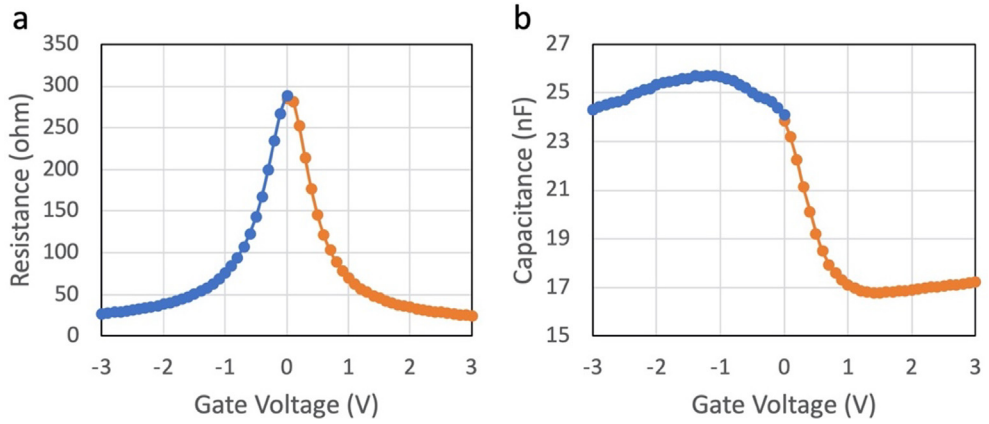


**Fig. 4.** (a) Resistance and (b) capacitance *vs.* gate voltage of the nanostructured MOS system with $Ga_2O_3$-in-glass active layer at 10 kHz of probing signal. Vertical error bars are within the symbol size. Uncertainty in the voltage value is less than the amplitude of the probing signal (100 mV) and is within the symbol size.

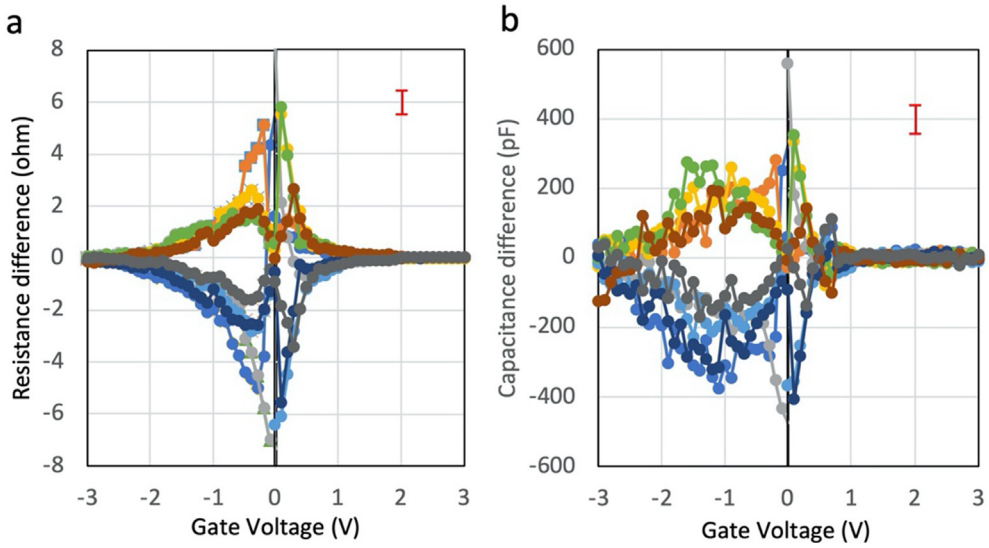


**Fig. 5.** Hysteretic *R* and *C* behavior. Difference in (a) resistance and (b) capacitance between ascending and previous descending ramps (warm colors, positive values) and descending and previous ascending ramps (cold colors, negative values) at negative or positive bias in nanostructured MOS system with $Ga_2O_3$-in-glass layer. Data are collected at 10 kHz of probing AC signal of 100 mV (similar data at different frequency are reported in Figure S3). Uncertainty in *R* and *C* values (less than 1%) is indicated by the red error bar. (For interpretation of the references to color in this figure legend, the reader is referred to the web version of this article.)

be described by a modification of the dielectric permittivity $\varepsilon_r$ of the oxide layer during the increase of negative bias. The change of $\varepsilon_r$ during the change of applied bias – caused by charge injection and charging of hard tracks – modifies in turn the *C-V* curve according to the change of capacitance response. The experimental curve can in fact be reproduced by a collection of values belonging to curves which describe responses of the unblocked system at different charged states (Fig. 6). These curves are obtained by modifying a reference curve – which models the limit *C* values in accumulation and inversion regime in unblocked conditions – through a bias dependent $\varepsilon_r(V)$ dielectric permittivity. In other words, the capacitance value at a specific bias is obtained as a deviation from the unblocked limit response calculated from *C* values at large bias, where the deviation arises from a modified permittivity, which in turn reflects the charge state of the system. This kind of effect appears to account for both the anomalous bump of the *C-V* curve at intermediate negative bias and the experimental hysteretic behavior (inset in Fig. 6). According to the model, nanostructure charging prevails at low bias over charge draining, and the dipole formation enhances the dielectric permittivity of the oxide layer. When the bias is instead high enough for draining charge over the nanostructure barrier, the system approaches the unblocked condition, and $\varepsilon_r$ recovers its unperturbed value. However, the backward process does not proceed along the same charging/discharging steps, because it starts from unblocked conditions and moves to lower electric fields unable to overcome Coulombic barriers. As a result, the process is hysteretic. It is worth noting that the capacitance response appears not to involve localized charge trapping in the layer or at the interfaces, since no relevant shift of the flat band voltage does follow the observed hysteretic response – as instead observed in other nanostructured oxides [35,36] – probably for a specific role of composition and/or nanophase concentration.

### 3.2. Plastic response to pulsed electric stimulus

A hysteretic behavior is a promising premise, in general, for a plastic response to occur. However, a plastic response must also imply that the irreversible mechanism responsible for hysteresis does not recover the system to the initial conditions at the end of the stimulus. In the case where responsivity is based on competitive mechanisms of nanostructure charging and charge hopping between nanoparticles, the electrostatics at null bias is important in determining an uncomplete recovery of the pristine conditions after cycles of electric stress. Specifically, a plastic response can be favored in a chargeable nanostructured system when the irreversible charging after a bias cycle, or a pulse, keeps memory of previous stimuli in the subsequent response.

Preliminary evidence of a plastic response from this type of mechanism can indeed be found in the nanostructured MOS here investigated. The system displays modifications, for several s, of both capacitance and resistance at the end of stimuli of 5 V, measured at null bias by an AC probe of 0.1 V, with duration of a few s (Figs. S4, S5). The experiments include different types of pulsed stimuli, comprising single negative or positive pulses, symmetric pulses – either positive/negative and negative/positive pulses – and train of two pulses with different combination of sign (Fig. S6).

Importantly, capacitance and resistance modifications – collected in several experiments – shade a mutual dependence which resembles that described by Eq. (6) and Fig. 2. The lowering of *R* after stimulus is in fact accompanied by a lowering of C and viceversa, as expected by charge transport events which involve opening or blocking of conduction channels in a percolative network able to accumulate electric charge in nanostructures. This result appears to be first evidence of a real potential of nanostructured

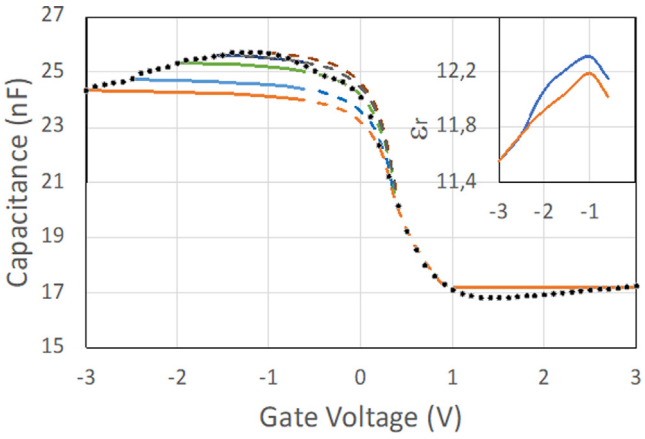


**Fig. 6.** Experimental *C-V* response of the nanostructured MOS (dots) compared with the expected response in the approximation of unblocked conduction channels (full line) at progressively charged states of nanostructures (from low to high charge states at increasing *C* values) modelled by increasing the dielectric permittivity to account for dipole formation. Inset: dielectric permittivity values reproducing the experimental curve at increasing (blue) and decreasing (orange) negative bias. Dashed lines are guides for the eye in the region which cannot be described within the unblocked model. Uncertainty in *C* is less than 1%. (For interpretation of the references to color in this figure legend, the reader is referred to the web version of this article.)

oxide layers as responsive systems with a plastic response related to mechanisms of charge transport and remanent accumulation.

Interestingly, changes of capacitance and resistance after stimulus – with respect to pristine values – are only registered when the last bias of the stimulus is positive (at duration longer than 1 s), no matter what the combination of pulses is (Fig. 7).

The asymmetry of responsivity with respect to the bias – which reflects the asymmetry of the MOS system, whose estimated flat band voltage is in fact negative – open the way to structures with design selective responsivity.

The plastic response in Fig. 7 indeed shows additional features which deviate from the expected mutual competitive dependence of Eq. (6) and point to a quite more complex response in the mate-

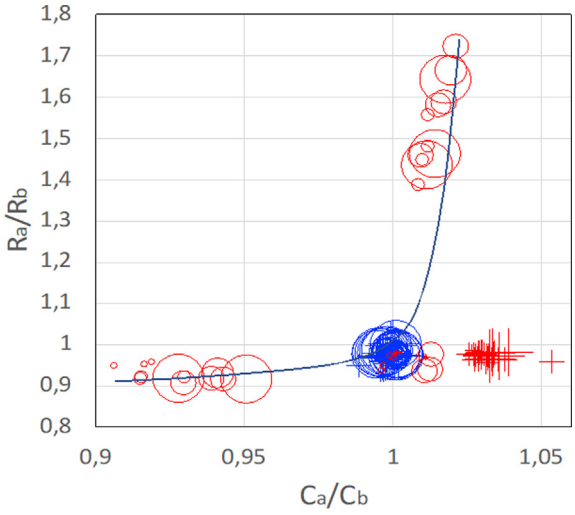


**Fig. 7.** Results from pulsed experiments. Ratio $R_a/R_b$ between resistance after and before pulsed stimulus *vs.* ratio $C_a/C_b$ between capacitance after and before pulsed stimulus with positive bias (red marks) or negative bias (blue marks) in the final part of the stimulus, either at 6 kHz (crosses) or 600 kHz (circles) of probing field. Mark sizes are proportional to the duration of the final bias of the pulse train, from 1 to 8 s. The line is a guide for the eye. (For interpretation of the references to color in this figure legend, the reader is referred to the web version of this article.)

rial with respect to the model. Namely, deviations from the model are found in the data collected at relatively low frequency below 10 kHz – which do not follow the expected large increase of resistance with capacitance increase (red crosses in Fig. 7) – and in the quantitative decrease of resistance at decreasing capacitance, which is less relevant than expected. Such features, in the specific material, could indeed result from the occurrence of concomitant charge transport mechanisms with different characteristic time [26] (which could be the reason of a different response at low frequency), and from nanostructure charging which could influence and block not only one but a multiplicity of conduction channels (with a resulting resistance recovery lower than expected at relatively large capacitance recovery).

## 4. Conclusions

The present work suggests a real potential of nanostructured oxides as responsive systems, shedding some light to the main mechanisms which can make a plastic response feasible in this class of materials. Namely, the idea that competitive processes of charge transport and accumulation could give rise to a plastic electric response in a randomly nanostructured oxide receives here a first analysis and a preliminary proof of concept on a real system.

The present study clarifies and models how a responsive and plastic behavior can occur in such systems because of concomitant effects, comprising i) electric field dependent conductivity, ii) bias dependent capacitance, iii) hysteretic behavior of resistance and capacitance, together with iv) remanent effects of the hysteretic response at null bias.

The study shows that these effects are expected when specific structural and physical features occur in the system, namely, i) nanostructure-mediated electric conduction, ii) chargeable nanostructure phases, iii) random distribution of nanostructure sizes and/or relative distances, and iv) asymmetric response to an external bias.

The investigated material system – thanks to its randomly nanostructured features within an oxide-in-oxide material – does indeed give preliminary but clear evidence of the predicted properties, including, respectively, i) bias-dependent resistance-lowering by an order of magnitude within 2 V, ii) bias dependent capacitance in accumulation regime, ascribable to charge accumulation within the nanostructured oxide layer and consequent change of dielectric permittivity, iii) hysteretic resistance and capacitance along bias cycles, and iv) resistance and capacitance changes after pulsed stimuli with respect to pristine values, dependent on bias sign, value, and duration.

In summary, the reported data and their interpretation give first feedback about the feasibility of an unprecedented strategy for the design of responsive devices based on a new concept of plastic response in randomly nanostructured fully dielectric materials.

## Data availability

Data will be made available on request.

## Declaration of Competing Interest

The authors declare that they have no known competing financial interests or personal relationships that could have appeared to influence the work reported in this paper.

## Acknowledgment

This work is partly supported by the Mendeleev University of Chemical Technology [Project no. 2020-036, 2020].

## Appendix A. Supplementary material

Supplementary data to this article can be found online at https://doi.org/10.1016/j.matdes.2023.111825.

## References

[1] K. Berggren et al., Roadmap on emerging hardware and technology for machine learning, Nanotechnology 32 (2020) 012002.
[2] T.-T. Liu, Y.-H. Zhu, J.-C. Shu, M. Zhang, M.-S. Cao, Patterned MXene-enabled switchable health monitoring and electromagnetic protection for architecture, Mater. Today Phys. 31 (2023) 100988.
[3] J.-C. Shu, M.-S. Cao, Y.-L. Zhang, Y.-Z. Wang, Q.-L. Zhao, X.-Y. Fang, S.-H. Yang, Y. Qin, J. Yuan, Atomic-molecular engineering tailoring graphene microlaminates to tune multifunctional antennas, Adv. Funct. Mater. 2212379 (2023).
[4] M.-S. Cao, X.-X. Wang, M. Zhang, W.-Q. Cao, X.-Y. Fang, J. Yuan, Variable-temperature electron transport and dipole polarization turning flexible multifunctional microsensor beyond electrical and optical energy, Adv. Mater. 32 (2020) 1907156.
[5] T. Guo, B. Sun, S. Ranjan, Y. Jiao, L. Wei, Y.N. Zhou, Y.A. Wu, From memristive materials to neural networks, ACS Appl. Mater. Interfaces 12 (2020) 54243–54265.
[6] Tie Zhang, Ke Xu, Jie Li, Lei He, Da-Wei Fu, Qiong Ye, Ren-Gen Xiong, Ferroelectric hybrid organic–inorganic perovskites and their structural and functional diversity, Natl Sci Rev 10 (2023) nwac240.
[7] F.u. Da-Wei, J.-X. Gao, P.-Z. Huang, R.-Y. Ren, T. Shao, L.-J. Han, J. Liu, J.-M. Gong, Observation of transition from ferroelasticity to ferroelectricity by solvent selective effect in anilinium bromide, Angew. Chem. Int. Ed. 60 (2021) 8198–8202.
[8] H.-G. Hwang, J.-U. Woo, T.-H. Lee, S.-M. Park, T.-G. Lee, W.-H. Lee, S. Nahm, Synaptic plasticity and preliminary-spike-enhanced plasticity in a CMOS-compatible $Ta_2O_5$ memristor, Mater. Design 187 (2020) 108400.
[9] Z. Chen, Y. Yu, L. Jin, Y. Li, Q. Li, T. Li, Y. Zhang, H. Dai, J. Yao, Artificial synapses with photoelectric plasticity and memory behaviors based on charge trapping memristive system, Mater. Design 188 (2020) 108415.
[10] S.-M. Park, H.-G. Hwang, J.-U. Woo, W.-H. Lee, S.-J. Chae, S. Nahm, Improvement of conductance modulation linearity in a $Cu^{2+}$-Doped $KNbO_3$ memristor through the increase of the number of oxygen vacancies, ACS Appl. Mater. Interfaces 12 (1) (2020) 1069–1077.
[11] A.C. Khot, N.D. Desai, K.V. Khot, M.M. Salunkhe, M.A. Chougule, T.M. Bhave, R.K. Kamat, K.P. Musselman, T.D. Dongale, Bipolar resistive switching and memristive properties of hydrothermally synthesized $TiO_2$ nanorod array: effect of growth temperature, Mater. Design 151 (2018) 37–47.
[12] Z. Ma, J. Ge, W. Chen, X. Cao, S. Diao, Z. Liu, S. Pan, Reliable memristor based on ultrathin native silicon oxide, ACS Appl. Mater. & Interfaces 14 (18) (2022) 21207–21216.
[13] B. Qu, H. Du, T. Wan, X. Lin, A. Younis, D. Chu, Synaptic plasticity and learning behavior in transparent tungsten oxide-based memristors, Mater. Design 129 (2017) 173–179.
[14] J. Ge, H. Huang, Z. Ma, W. Chen, X. Cao, H. Fang, J. Yan, Z. Liu, W. Wang, S. Pan, A sub-500 mV monolayer hexagonal boron nitride based memory device, Mater. Design. 198 (2021) 109366.
[15] A.A. Gismatulin, V.A. Voronkovskii, G.N. Kamaev, Y.N. Novikov, V.N. Kruchinin, G.K. Krivyakin, V.A. Gritsenko, I.P. Prosvirin, A. Chin, Electronic structure and charge transport mechanism in a forming-free $SiO_x$-based memristor, Nanotechnology 31 (2020) 505704.
[16] Y. Li, E.J. Fuller, S. Asapu, S. Agarwal, T. Kurita, J.J. Yang, A.A. Talin, Low-voltage, CMOS-free synaptic memory based on $Li_XTiO_2$ redox transistors, ACS Appl. Mater. Interfaces 11 (42) (2019) 38982–38992.
[17] J.-H. Cha, S.Y. Yang, J. Oh, S. Choi, S. Park, B.C. Jang, W. Ahna, S.-Y. Choi, Conductive-bridging random-access memories for emerging neuromorphic computing, Nanoscale 12 (2020) 14339–14368.
[18] Y. Zhu, J.-S. Liang, V. Mathayan, T. Nyberg, D. Primetzhofer, X. Shi, Z. Zhang, High performance full-inorganic flexible memristor with combined resistance-switching, ACS Appl. Mater. Interfaces 14 (18) (2022) 21173–21180.
[19] M. Talaeizadeh, L. Jamilpanah, S.A. Seyed Ebrahimi, S.M. Mohseni, Resistive switching characteristics of $Co_2FeSi$ and Mn with $Al_2O_3$ granular nanocomposites, J. Magn. Magn. Mater. 516 (2020) 167336.
[20] M. Kim, M.A. Rehman, D. Lee, Y. Wang, D.-H. Lim, M.F. Khan, H. Choi, Q.Y. Shao, J. Suh, H.-S. Lee, H.-H. Park, Filamentary and interface-type memristors based on tantalum oxide for energy-efficient neuromorphic hardware, ACS Appl. Mater. Interfaces 14 (39) (2022) 44561–44571.
[21] S. Kim, H. Kim, S. Hwang, M.-H. Kim, Y.-F. Chang, B.-G. Park, Analog synaptic behavior of a silicon nitride memristor, ACS Appl. Mater. Interfaces 9 (46) (2017) 40420–40427.
[22] W. Zhou, R. Yang, H.-K. He, H.-M. Huang, J. Xiong, X. Guo, Optically modulated electric synapses realized with memristors based on ZnO nanorods, Appl. Phys. Lett. 113 (2018) 061107/1-5.
[23] Y. Zhu, J.-S. Liang, X. Shi, Z. Zhang, Full-Inorganic Flexible $Ag_2S$ Memristor with Interface Resistance-Switching for Energy-Efficient Computing, ACS Appl. Mater. Interfaces 14 (38) (2022) 43482–43489.
[24] A. Paleari, S. Brovelli, R. Lorenzi, M. Giussani, A. Lauria, N. Mochenova, N. Chiodini, Tunable dielectric function in electric-responsive glass with tree-like

percolating pathways of chargeable conductive nanoparticles, Adv. Functional Mater. 20 (2010) 3511–3518.
[25] S. Brovelli, N. Chiodini, R. Lorenzi, A. Lauria, M. Romagnoli, A. Paleari, Fully inorganic oxide-in-oxide ultraviolet nanocrystal light emitting devices, Nature Commun. 3 (1) (2012) 1–9.
[26] J. Remondina, A. Paleari, N.V. Golubev, E.S. Ignat'eva, V.S. Sigaev, M. Acciarri, S. Trabattoni, A. Sassella, R. Lorenzi, Responsive charge transport in wide-band-gap oxide films of nanostructured amorphous alkali-gallium-germanosilicate, J. Mater. Chem. C 7 (2019) 7768–7778.
[27] J. Remondina, S. Trabattoni, A. Sassella, N.V. Golubev, E.S. Ignat'eva, V.N. Sigaev, M. Acciarri, B. Schrode, R. Resel, A. Paleari, R. Lorenzi, Lenticular Ga-oxide nanostructures in thin amorphous germanosilicate layers - Size control and dimensional constraints, Mater. Des. 204 (2021) 109667.
[28] N.F. Mott, E.A. Davis, Electron process in non-crystalline materials, Claredon Press, Oxford, 1979.
[29] R.A. Marcus, On the Theory of Electron-Transfer Reactions. VI. Unified Treatment for Homogeneous and Electrode Reactions, J. Chem. Phys. 43 (1965) 679–701.
[30] Y.A. Berlin, M.A. Ratner, Intra-molecular electron transfer and electric conductance via sequential hopping: Unified theoretical description, Radiation Phys. Chem. 74 (2005) 124–131.
[31] M. Reato, T. Dainese, S. Antonello, F. Maran, Electron transfer in films of atomically precise gold nanoclusters, Chem. Mater. 33 (2021) 4177–4187.
[32] P. Zukowski, T.N. Koltunowicz, O. Boiko, V. Bondariev, K. Czarnacka, J.A. Fedotova, A.K. Fedotov, I.A. Svito, Impedance model of metal-dielectric nanocomposites produced by ion-beam sputtering in vacuum conditions and its experimental verification for thin films of (FeCoZr)x(PZT)(100–x), Vacuum 120 (2015) 37–43.
[33] M. Houssat, C. Villeneuve-Faure, N. Lahoud Dignat, J.-P. Cambronne, Nanoscale mechanical and electrical characterization of the interphase in polyimide/silicon nitride nanocomposites, Nanotechnology 32 (2021) 425703.
[34] M. Niklaus, H.R. Shea, Electrical conductivity and Young's modulus of flexible nanocomposites made by metal-ion implantation of polydimethylsiloxane: The relationship between nanostructure and macroscopic properties, Acta Mater. 59 (2011) 830–840.
[35] I. Crupi, S. Lombardo, C. Spinella, C. Bongiorno, Y. Liao, C. Gerardi, B. Fazio, M. Vulpio, S. Privitera, Electrical and structural characterization of metal–oxide–semiconductor capacitors with silicon rich oxide, J. Appl. Phys. 89 (2001) 5552–5558.
[36] S.V. Mahajan, J.H. Dickerson, Dielectric properties of colloidal $Gd_2O_3$ nanocrystal films fabricated via electrophoretic deposition, Appl. Phys. Lett. 96 (2010) 113105.
[37] V.N. Sigaev, N.V. Golubev, E.S. Ignat'eva, B. Champagnon, D. Vouagner, E. Nardou, R. Lorenzi, A. Paleari, Native amorphous nanoheterogeneity in gallium germanosilicates as a tool for driving $Ga_2O_3$ nanocrystal formation in glass for optical devices, Nanoscale 2013, 5, 299-306.
[38] H.Y. Playford, A.C. Hannon, M.G. Tucker, D.M. Dawson, S.E. Ashbrook, R.J. Kastiban, J. Sloan, R.I. Walton, Characterization of Structural Disorder in γ-$Ga_2O_3$, J. Phys. Chem. C 118 (2014) 16188.
[39] K. Tang, A.C. Meng, R. Droopad, P.C. McIntyre, Temperature dependent border trap response produced by a defective interfacial oxide layer in $Al_2O_3$/InGaAs gate stacks, ACS Appl. Mater. Interfaces 8 (44) (2016) 30601–30607.
[40] L. Binet, D. Gourier, Origin of the blue luminescence of β -$Ga_2O_3$, J. Phys. Chem. Solid 59 (1998) 1241.
[41] T. Wang, P.V. Radovanovic, In situ enhancement of the blue photoluminescence of colloidal $Ga_2O_3$ nanocrystals by promotion of defect formation in reducing conditions, Chem. Commun. 47 (2011) 7161–7163.
[42] M. Fogler, S. Teber, B. Shklovskii, Variable-range hopping in quasi-one-dimensional electron crystals, Phys. Rev. B: Condens. Matter Mater. Phys. 69 (2004) 035413.
[43] P. Sheng, Fluctuation-induced tunneling conduction in disordered materials, Phys. Rev. B: Condens. Matter Mater. Phys. 21 (1980) 2180–2195.
[44] C. Filipič, A. Levstik, Z. Kutnjak, P. Umek, D. Arčon, Fluctuation-induced tunneling in $TiO_2$-derived nanotube pellets, J. Appl. Phys. 101 (2007) 084308.
[45] P. Sheng, E. Sichel, J. Gittleman, Fluctuation-induced tunneling conduction in carbon-polyvinylchloride composites, Phys. Rev. Lett. 40 (1978) 1197–1200.
[46] A. Paleari, V.N. Sigaev, N.V. Golubev, E.S. Ignat'eva, A. Azarbod, R. Lorenzi, Crystallization of nano-heterogeneities in Ga-containing germanosilicate glass: dielectric and refractive response changes, Acta Mater. 70 (2014) 19–29.